https://doi.org/10.3311/PPch.45067
Creative Commons Attribution

Periodica Polytechnica Chemical Engineering

Natural Calcite-Rich Limestone for Lead(II) Immobilization from Mining-Impacted Waters: Insights into the Removal Mechanism

Bojana Knežević Vulićević[1*], Vlatko Kastratović[2], Jana Mišurović[3], Milica Kosović Perutović[3], Aleksandra Gezović Miljanić[3]

[1] Centre for Ecotoxicological Research Podgorica, Bulevar Šarla de Gola 2, 81000 Podgorica, Montenegro
[2] Department of Chemistry, Faculty of Natural Sciences and Mathematics, University of Montenegro, Bulevar Džordža Vašingtona bb., 81000 Podgorica, Montenegro
[3] Faculty of Technology, University of Montenegro, Bulevar Džordža Vašingtona bb., 81000 Podgorica, Montenegro
[*] Corresponding author, e-mail: bojana.knezevic@ceti.me

Received: 08 June 2026, Accepted: 15 September 2026, Published online: 11 November 2026

Abstract

Using naturally available and low-cost materials for the removal of toxic metals from contaminated waters has long been recognized as a promising and sustainable approach. This study evaluates the potential of calcite-rich natural limestone from the "Šuplja Stijena" stone deposit (Pljevlja, Montenegro) for Pb(II) removal from aqueous solutions and acid mine drainage. Batch experiments demonstrated that Pb(II) removal is strongly influenced by the solid-to-liquid ratio, particle size, pH, and initial metal concentration. The highest experimental uptake reached 310 mg/g at an initial Pb(II) concentration of 900 mg/L, with a removal efficiency of 86%. Kinetic analysis revealed two distinct removal stages, indicating that a single adsorption mechanism cannot adequately describe the overall process. Time-resolved *ex-situ* Fourier transform infrared and X-ray diffraction analyses showed that the transition between these kinetic stages is accompanied by the structural evolution of the sorbent, involving initial surface interactions followed by partial calcite dissolution, Ca^{2+}/Pb^{2+} ion exchange and progressive cerussite ($PbCO_3$) formation. Although the Langmuir and Freundlich models yielded high correlation coefficients, the obtained parameters lacked physical significance, suggesting that classical equilibrium adsorption isotherms provide only a limited description of this complex removal process. Experiments performed with real acid mine drainage further confirmed the applicability of the investigated limestone under environmentally relevant conditions. These findings demonstrate that locally available calcite-rich limestone overburden is an effective and inexpensive material for Pb(II) removal while providing mechanistic insight into the coupled processes governing metal immobilization.

Keywords

acid mine drainage, adsorption, calcite-rich limestone, lead, adsorption capacity

1 Introduction

The removal of metal ions from contaminated waters by adsorption onto natural materials and rocks has attracted considerable attention as an economical, simple, and efficient remediation approach [1–4]. This method has been widely investigated for heavy metal removal due to the availability of low-cost adsorbents and its operational simplicity [5]. The success of using adsorption in industrial effluent decontamination processes depends largely on the choice of an efficient, inexpensive adsorbent that has high stability (mechanical and chemical) [6]. However, various forms of even the same minerals and rocks reflect different geological conditions and tectonic effects, which influence their morphology, physicochemical properties, and crystallinity [7, 8]. Consequently, calcite in the natural environment exhibits significant variations in color, chemical composition, microstructural deformation, and degree of crystallinity [7, 9].

The interaction of calcite with dissolved metal ions involves adsorption processes and redox reactions [8–10]. Metal ions can be incorporated into calcite, causing significant defects in the crystal structure, which have a major impact on chemical reactivity, optical, mechanical, and electronic properties [10, 11]. Several studies have shown

Cite this article as: Knežević Vulićević, B., Kastratović, V., Mišurović, J., Kosović Perutović, M., Gezović Miljanić, A. "Natural Calcite-Rich Limestone for Lead(II) Immobilization from Mining-Impacted Waters: Insights into the Removal Mechanism", Periodica Polytechnica Chemical Engineering, 2026. https://doi.org/10.3311/PPch.45067

that temperature, pH, and the molar ratio of metal to Ca ions control the incorporation of foreign ions into calcite [12].

Although the interaction between calcite and Pb(II) ions has been widely investigated, many studies have been performed using pure, commercial, or simplified calcite-based systems under controlled laboratory conditions. Natural calcite materials, however, may exhibit different adsorption behavior due to variations in mineralogical composition, crystallinity, surface properties, and the presence of associated mineral phases. Therefore, further investigation of locally available natural calcite materials under more complex conditions, including real mine waters containing multiple dissolved components, is still needed. Calcite was selected as an adsorbent because it is one of the most abundant carbonate minerals, environmentally compatible, and capable of immobilizing heavy metals through surface adsorption and precipitation reactions. Pb(II) was selected as a target contaminant due to its high toxicity, persistence in aquatic environments, and frequent occurrence in mining-affected waters.

Several studies have demonstrated the ability of calcite-based materials to immobilize Pb(II) through a combination of adsorption, ion exchange, and surface precipitation mechanisms. Fiorito et al. [12] reported that commercial calcite promotes heterogeneous nucleation and surface coprecipitation of Pb phases, while Alkhatib et al. [13] showed that pure calcite exhibited faster Pb(II) uptake compared with calcitic soil due to the greater availability of active adsorption sites. Other studies have emphasized the influence of associated minerals and organic matter on Pb immobilization, demonstrating that the adsorption efficiency depends strongly on the composition and structure of the calcite-based material [14].

In this study, the potential application of a natural calcite-rich limestone material for Pb(II) adsorption was investigated using kinetic and adsorption models to quantify adsorption capacity and evaluate the influence of competing metal ions. The novelty of this study lies in the evaluation of a locally available natural calcite material using both synthetic solutions and real mine waters, combined with detailed mineralogical characterization. This approach gives insight into the applicability of natural calcite under conditions closer to those encountered in contaminated mining environments.

2 Materials and methods

2.1 Materials

2.1.1 Calcite material

Natural limestone samples used in this study were collected from natural deposits in the exploitation area of the "Šuplja Stijena" lead and zinc mine in the municipality of Pljevlja (Montenegro). Although the bulk material originates from limestone overburden, mineralogical characterization by X-ray diffraction (XRD) and Fourier transform infrared spectroscopy (FTIR) performed in this work (Section 3.3.1) confirmed that calcite is the dominant mineral phase. Therefore, the term limestone is used throughout this work when referring to the natural material used in experiments, whereas calcite refers to the dominant mineral phase identified in the material and is used when discussing the mechanisms of Pb(II) removal. The samples were first crushed using a crushing plant and then sieved with a combination of different mesh sizes. In this way, three calcite fractions were obtained: coarse (16–23 mm), medium (8–16 mm), and fine (4–8 mm). These fractions were used for experiments in a flow-through system with real samples of acidic mine water.

Samples of the limestone material intended for laboratory tests were prepared by grinding the fine fraction (4–8 mm) in a ball mill (Centrifugal Ball Mill S 100, Retsch GmbH, Germany), followed by sieving through a series of sieves (Woven Wire Mesh Sieves, Retsch GmbH, Germany). Four particle size fractions were prepared for testing: <0.5 mm, 0.5–1 mm, 1–2 mm, and 2–4 mm. After sieving, fractions larger than 0.5 mm were washed with deionized water to remove smaller particles that may have remained on the surface during sieving and then air-dried.

Characterization of the tested material before and after adsorption was performed using XRD and FTIR. Diffractograms were measured on a Rigaku MiniFlex 600-C X-ray diffractometer (Rigaku Corporation, Japan) operating at 40 kV and 15 mA in parafocusing Bragg-Brentano geometry, where Cu-Kα radiation was paired with a D/teX Ultra2 MF direct-detection semiconductor-strip detector. A single-crystal silicon was used as material support, and diffractograms were recorded with a step size of 0.01° and a data acquisition rate of 2°/min. FTIR spectra were recorded with a PerkinElmer Spectrum Two FT-IR spectrometer (PerkinElmer, USA) in reflection mode using the attenuated total reflectance (ATR) technique on a diamond crystal, in wavenumber range 4000–400 cm^{-1} with 16 scans per spectrum and at a resolution of 2 cm^{-1}.

2.1.2 Model solutions of lead ions

Adsorption experiments were conducted using model solutions of heavy metals prepared by diluting commercially available standard solutions of the lead (CPA Chem, Bulgaria). Ultra-pure deionized water (18.2 MΩ) produced by a GenPure water purification system (Thermo Fisher Scientific, USA) was used for the preparation of

all solutions. Binary solutions used in the competing-ion experiments (Section 2.2.3) were prepared from single-element standard solutions of Cd, Ni, Cu, Cr, Zn, Mn, Fe, Al and As (CPA Chem, Bulgaria), all in nitrate form except As (As_2O_3). Ethylenediaminetetraacetic acid disodium salt dihydrate ($Na_2EDTA{\cdot}2H_2O$, ACS reagent, ≥ 99%, Sigma Aldrich, Germany) was used to prepare the 0.0025 M and 0.01 M EDTA solutions for the desorption experiments.

2.1.3 Real water samples

The adsorption efficiency of the calcite material for the removal of lead was also evaluated using real water samples. Water sampling was performed three times, in September 2023, 2024, and 2025, from the Mjedenički stream at a location downstream of the "Šuplja Stijena" open pit – downstream of waters originating from abandoned mine shafts. The water samples were collected and transported to the laboratory in accordance with the guidelines of the standard methods MEST EN ISO 5667-1:2023 [15] and MEST EN ISO 5667-6:2017 [16]. The samples were not preserved. At the endpoint of the experiment, a water sample was collected, filtered, and analyzed for dissolved lead concentration.

2.2 Experimental procedure

2.2.1 Batch experiments

Pb(II) removal experiments were performed in 50 mL tubes. Synthetic Pb^{2+} solutions were used as the aqueous phase for the adsorption experiments. All experiments were conducted at room temperature and performed in triplicate, and the reported values represent the average of three independent measurements. Experimental reproducibility was evaluated by calculating the relative standard deviation (RSD). Lead determination was performed according to the standard ICP-OES method ISO 11885:2007 [17], validated for the determination of lead in water. The accuracy of the method was confirmed by a recovery rate of 98%, while the precision, expressed as the repeatability relative standard deviation (RSD), was 2.4%. Quality assurance and quality control (QA/QC) procedures included calibration verification using an independent control standard after each calibration, analysis of the control standard after every ten samples, and analysis of procedural blanks to monitor potential contamination throughout the analytical procedure. After a defined contact time, the suspension was filtered, and the filtrate was analyzed for Pb^{2+} ion concentration. From the material balance, the amount of adsorbed metal, adsorption capacity, and its change with adsorption time were determined.

The removal efficiency (R, %) and adsorption capacity (q_e, mg/g) were calculated using Eqs. (1) and (2) [18]:

$$R = \frac{c_0 - c_e}{c_0} \cdot 100, \tag{1}$$

$$q_e = \frac{(c_0 - c_e)V}{m}, \tag{2}$$

where R (%) is the removal efficiency, q_e (mg/g) is the adsorption capacity, c_0 and c_e (mg/L) are the initial and equilibrium concentrations of lead in solution, respectively, m (g) is the adsorbent mass and V (L) is the solution volume. For kinetic experiments, c_e and q_e are replaced by c_t and q_t, the values at contact time t.

A batch adsorption procedure was applied to investigate the optimal adsorbent mass and particle size, equilibrium time, effective pH value, and the influence of the initial metal concentration on adsorption.

All batch experiments were performed with 40 mL solution at room temperature (22 ± 2 °C) and a shaking speed of 100 rpm on a horizontal shaker (HS 501 digital, IKA Werke, Germany). Two series of experiments were carried out:

1. *Optimization of operating parameters*: the effects of adsorbent mass (0.01–1 g), particle size (< 0.5 mm to 2–4 mm), contact time (0.5–15 min) and initial pH (2–6) were studied at a low initial Pb(II) concentration of 5 mg/L, which is representative of contaminated natural waters. Only one parameter was varied at a time, while the others were kept constant at limestone mass 1 g, particle size 1–2 mm, pH 5.00 and contact time 15 min.
2. *Isotherm and kinetic experiments*: these were performed under the conditions selected in series '1.' above within this listing (0.1 g limestone, particle size < 0.5 mm, pH 5). The adsorbent mass was reduced to 0.1 g and the initial Pb(II) concentration was increased to 900–6750 mg/L in order to approach saturation of the adsorption sites (see Section 3.1.2). Kinetic experiments were performed at an initial Pb(II) concentration of 1455 mg/L with contact times of 5–960 min.

After filtration through 0.45 μm PTFE filter (Amtast China) dissolved lead concentration was determined by inductively coupled plasma optical emission spectrometry (ICP-OES, iCAP Duo 7400, Thermo Fisher Scientific, USA).

2.2.2 Adsorption isotherms and adsorption kinetics

The isotherm data were analysed using the Langmuir [19, 20] and Freundlich [21] models, and the adsorption kinetics were

evaluated using the pseudo-first-order [22] and pseudo-second-order [23] kinetic models. The linear forms of the models are given in Eqs. (3) to (7) and are also summarized in Table A1 (Appendix A).

The Langmuir model assumes monolayer adsorption on a finite number of energetically equivalent sites without interaction between adsorbed species. Its linear form is:

$$\frac{c_e}{q_e} = \frac{1}{K_L q_{\max}} + \frac{c_e}{q_{\max}}, \tag{3}$$

where $q_{\max}$ (mg/g) is the maximum (monolayer) adsorption capacity, and K_L (L/mg) is the Langmuir constant related to the affinity of the binding sites. $q_{\max}$ and K_L were obtained from the slope ($1/q_{\max}$) and the intercept ($1/(K_L\, q_{\max})$) of the plot of c_e/q_e *versus* c_e.

The favourability of adsorption was assessed using the dimensionless separation factor R_L [20]:

$$R_L = \frac{1}{1 + K_L c_0}. \tag{4}$$

Adsorption is favourable for $0 < R_L < 1$, unfavourable for $R_L > 1$, linear for $R_L = 1$ and irreversible for $R_L = 0$. Since $K_L > 0$ by definition, physically meaningful values of R_L are always positive.

The Freundlich model describes adsorption on heterogeneous surfaces. Its linear form is:

$$\ln q_e = \ln K_F + \frac{1}{n} \ln c_e, \tag{5}$$

where K_F ((mg/g)(L/mg)$^{1/n}$) is the Freundlich constant related to adsorption capacity and $1/n$ (dimensionless) is the heterogeneity factor, which reflects adsorption intensity. Values of $0 < 1/n < 1$ indicate favourable adsorption.

The linear forms of the pseudo-first-order (PFO) and pseudo-second-order (PSO) kinetic models are:

$$\ln\left(q_e - q_t\right) = \ln q_e - k_1 t, \tag{6}$$

$$\frac{t}{q_t} = \frac{1}{k_2 q_e^2} + \frac{t}{q_e}, \tag{7}$$

where q_t (mg/g) is the adsorbed mass of Pb(II) per one gramm of sorbent at the given time t (min), k_1 (1/min) is the PFO rate constant and k_2 (g/(mg min)) is the PSO rate constant. The calculated equilibrium capacity $q_{e,calc}$ and the rate constants were obtained from the slopes and intercepts of the plots of $\ln(q_e - q_t)$ *versus* t and t/q_t *versus* t, respectively. The fitted parameters of all models are given in Table 1.

2.2.3 Effect of competing ions

In binary systems, combinations of the tested metals with lead were investigated under initial concentrations that provided approximately 50% removal efficiency for each component in single-component tests, in order to assess the individual effect of each metal on lead adsorption. This approach enables an evaluation of whether the presence of a specific metal enhances or hinders lead adsorption. Adsorption tests were conducted at pH 5, room temperature, using 0.1 g of limestone in 40 mL of solution. The initial concentrations of the elements in the binary solutions, added as single-element standard solutions (Section 2.1.2), were as follows: Cd^{2+} – 30 mg/L,

Table 1 Fitted parameters of the isotherm and kinetic models for lead(II) adsorption on limestone (0.1 g limestone, < 0.5 mm, 40 mL, pH 5, 22 ± 2 °C)

Model	Parameter	Value	R^2
Isotherms (c_0 = 900–6750 mg/L, t = 15 min)			
Langmuir, Eq. (3)	$q_{\max}$ (mg/g)	196	0.999
	K_L (L/mg)	−0.0076[a]	
	R_L	n.m.[a]	
Freundlich, Eq. (5)	K_F ((mg/g)(L/mg)$^{1/n}$)	555	
	$1/n$	−0.119[b]	0.987
Kinetics (c_0 = 1455 mg/L)	$q_{e,exp}$ (mg/g)	582[c]	
PFO, Eq. (6), t = 5–120 min	$q_{e,calc}$ (mg/g)	776	0.885
	k_1 (1/min)	0.0419	
PSO, Eq. (7), t = 5–120 min	$q_{e,calc}$ (mg/g)	765	0.967
	k_2 (g/(mg min))	3.39×10^{-5}	

[a] The negative intercept of the linear Langmuir plot gives a negative K_L, which has no physical meaning; R_L calculated from Eq. (4) would be negative (−0.17 to −0.02) and is therefore not meaningful (n.m.).
[b] A negative $1/n$ has no physical meaning within the Freundlich model.
[c] Experimental value at t = 960 min.

Ni^{2+} – 15 mg/L, Pb^{2+} – 1280 mg/L, Cu^{2+} – 30 mg/L, Cr^{3+} – 400 mg/L, Zn^{2+} – 75 mg/L, Mn^{2+} – 5 mg/L, Fe^{3+} – 50 mg/L, Al^{3+} – 150 mg/L and As^{3+} – 0.2 mg/L.

2.2.4 Desorption from the used material

To assess the potential for reusing the limestone adsorbent, as well as the risk of lead leaching from its surface, desorption experiments were conducted by bringing 0.1 g of limestone with adsorbed ions into contact with 40 mL of deionized water, rainwater, 0.0025 M EDTA and 0.01 M EDTA for a contact time of 16 h (shaking speed 100 rpm on a horizontal shaker). This approach was used to evaluate Pb(II) release from the calcite surface while minimizing the influence of calcite dissolution during the desorption process.

2.2.5 Adsorption of lead from real water samples

Batch adsorption experiments with real water samples were conducted in the same way as with model solutions, while additional tests of adsorption efficiency under real conditions were carried out in a flow-through system.

To evaluate the applicability of limestone material for metal adsorption under real conditions, acidic mine water samples were collected from the exploitation area of the "Šuplja Stijena" mine. Batch experiments were conducted under defined optimal conditions (1 g of limestone, 40 mL of water sample, 15 min contact time, 100 rpm). Since the main goal of this research is to develop a simple and cost-effective method for removing Pb^{2+} ions from contaminated waters, adsorption experiments were carried out at the natural pH of the sampled water without any additional pH adjustment.

The flow-through system consisted of a cylindrical column made of inert PVC material, equipped with a water reservoir, a pump for continuous circulation, a flow control valve, and inlet and outlet ports. The column was 1.5 m long, with an internal diameter of 110 mm, and was mounted on a stable stand at a 15° inclination to ensure uniform flow. The column was filled with 15 kg of calcite, and the total system capacity was 15 L of water. Experiments were conducted using three different calcite-rich limestone material fractions (coarse, medium and fine).

Since continuous monitoring of lead concentration was not possible within the system, pH was used as an indicator parameter. The initial pH of the tested water sample from Mjedenički stream was 3.0, and the endpoint of the experiment was defined as the moment when the pH reached 6.0, since this pH value represents the lower limit of the acceptable pH range for rivers according to the Rulebook on the manner and deadlines for determining the status of surface waters [24]. At that point, a water sample was collected and analyzed for the remaining lead content.

3 Results and discussion

3.1 Optimal conditions for lead removal

3.1.1 Effect of limestone mass, particle size, contact time and pH value

The effect of limestone mass on adsorption efficiency was investigated by testing eight different masses. The results (Fig. 1 (a)) show that removal efficiency (R) remains around 99–100% when the mass of limestone is ≥ 0.25 g, but decreases to 87% at 0.1 g and to 43% at 0.01 g. The adsorption capacity increases as the mass decreases, from 0.20 mg/g at 1 g to 8.6 mg/g at 0.01 g. The increase in removal efficiency up to an adsorbent mass of 0.25 g can be attributed to the increased availability of active sites with increasing solid dosage, while the lower adsorption capacity at higher dosages may result from the presence of excess adsorption sites that remain unsaturated and reduced utilization of adsorption sites [25].

The effect of particle size was studied in four size fractions (as mentioned in Section 2.1.1). A lower removal efficiency compared to the maximum was observed only for

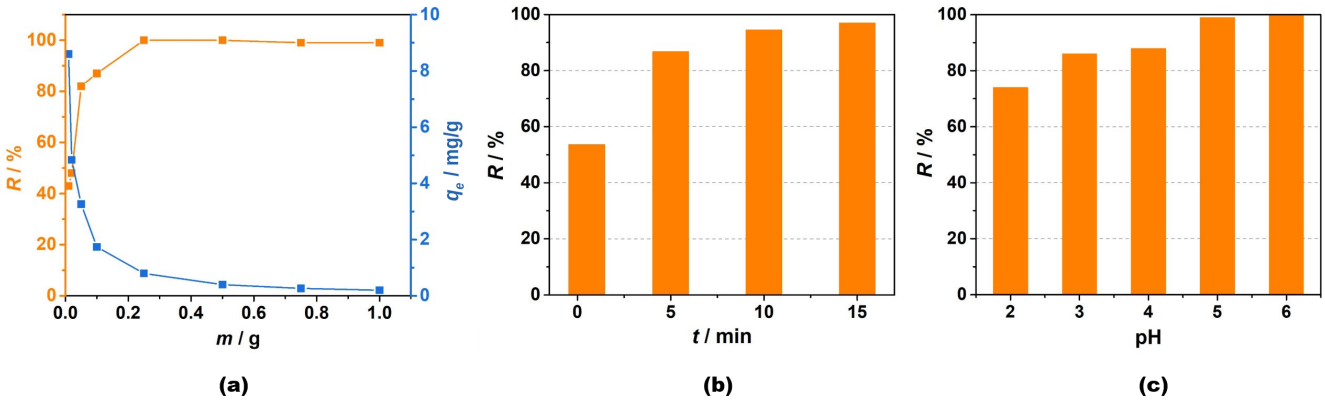


Fig. 1 Removal efficiency and adsorption capacity of lead(II) ions on limestone as a function of: (a) limestone mass; (b) contact time; (c) initial pH value (c_0 = 5 mg/L, 40 mL; mean values of three replicates; standard deviations are smaller than the symbol size)

the coarsest fraction (> 2 mm), where it reached 82%. This result is consistent with the well-known fact that increasing particle size reduces the contact surface area between the adsorbent and Pb^{2+} solution [26, 27], and consequently decreases the number of ions – exchangeable sites available for Pb^{2+} binding. The drop in efficiency is therefore mainly attributed to the reduced available surface area of calcite and the smaller number of accessible binding sites.

The effect of contact time on Pb^{2+} adsorption by calcite shows a very rapid initial adsorption. As shown on Fig. 1 (b) after only 30 s of contact under the tested conditions, the efficiency reached about 54%, increasing to 87% after 5 min and achieving nearly complete removal (98%) within 15 min. The high efficiency of calcite in Pb^{2+} removal within a relatively short period is consistent with the findings of Fadhel Ali et al. [28]. Similar results were reported for lead sorption on other materials [29–32]. Ibrahim et al. [33] showed that the sorption of Pb(II) onto biomass (dried water hyacinth) was rapid for the first 30 min, and equilibrium was reached within 60 min.

The adsorption process occurs in two stages [34]. The initial stage is rapid due to the high number of available active sites and the strong driving force caused by the high initial Pb^{2+} concentration. In the second stage, the number of free active sites decreases, and the residual Pb^{2+} concentration is lower, which significantly reduces the adsorption rate. Electrostatic repulsion may also occur due to the accumulation of a large number of cations [35]. In aqueous solutions, Pb^{2+} is the dominant ionic species below pH 4. As pH increases between 4 and 6, Pb^{2+} and $Pb(OH)^{+}$ coexist in approximately equal concentrations. At higher pH values, Pb^{2+} concentration decreases, and above pH 7, precipitation of $Pb(OH)_2$ becomes dominant, which may also exist in a partially hydrated form [36].

Experiments in this study were conducted up to pH 6, since above pH 5 lead transforms into insoluble hydroxide species, and the decrease in Pb^{2+} concentration can no longer be attributed solely to adsorption. The results show that adsorption efficiency increases with increasing pH. The lowest efficiency was observed at pH 2 (74%), while at pH 5 the efficiency reached 99% (Fig. 1 (c)). Lower efficiency in acidic conditions may result from competition between H^{+} ions and Pb^{2+} for active sites and from the positively charged adsorbent surface [37].

Based on the individual optimization results, the operating conditions selected for subsequent experiments were 0.1 g of limestone, particle size below 0.5 mm, pH 5, and a contact time of 15 min. The adsorbent mass of 0.1 g was selected based on the mass optimization study performed with the 0.5–1 mm particle fraction, where this amount achieved a Pb^{2+} removal efficiency of 87% while significantly reducing adsorbent consumption. Although higher adsorbent masses resulted in slightly higher removal efficiencies, their use would increase the amount of spent adsorbent generated without a proportional improvement in removal performance. The particle size below 0.5 mm was selected because the particle size study demonstrated enhanced Pb^{2+} removal efficiency with decreasing particle size, attributed to the larger available surface area and increased accessibility of adsorption sites. Therefore, these conditions were considered the most suitable for further investigations, providing a balance between removal efficiency and efficient use of the limestone material.

3.1.2 Effect of initial metal concentration and adsorption isotherms

Based on the previous results, the following initial Pb^{2+} concentrations were selected to investigate the effect of metal concentration on adsorption: 900, 1280, 1800, 4500, and 6750 mg/L. Experiments were carried out at pH 5 using 0.1 g of limestone (particle size < 0.5 mm), 40 mL of solution, room temperature, a stirring speed of 100 rpm, and a contact time of 15 min.

As shown in Fig. 2 (a), the removal efficiency decreased from 86% at an initial Pb^{2+} concentration of 900 mg/L to 7.4% at 6750 mg/L. This decrease can be attributed to the progressive saturation of the available adsorption sites as the Pb^{2+} concentration increased [37, 38]. In contrast, the amount of Pb(II) adsorbed per unit mass of limestone increased with increasing initial Pb(II) concentration because a higher initial concentration provides a greater driving force for mass transfer of Pb^{2+} ions from the solution to the adsorbent surface [39]. However, the adsorption capacity calculated at equilibrium (q_e) gradually decreased from 310 to approximately 200 mg/g, indicating that the available adsorption sites became increasingly occupied at higher metal concentrations.

The investigation of the initial lead concentration is important because contaminated waters may contain lead over a broad concentration range depending on their origin. Understanding the influence of the initial concentration enables optimization of the adsorbent dosage and improves the practical application of limestone in batch treatment systems.

For the adsorption isotherm study, the same concentration range (900–6750 mg/L) was selected. Preliminary experiments performed at lower lead concentrations resulted in removal efficiencies exceeding 90%, providing insufficient

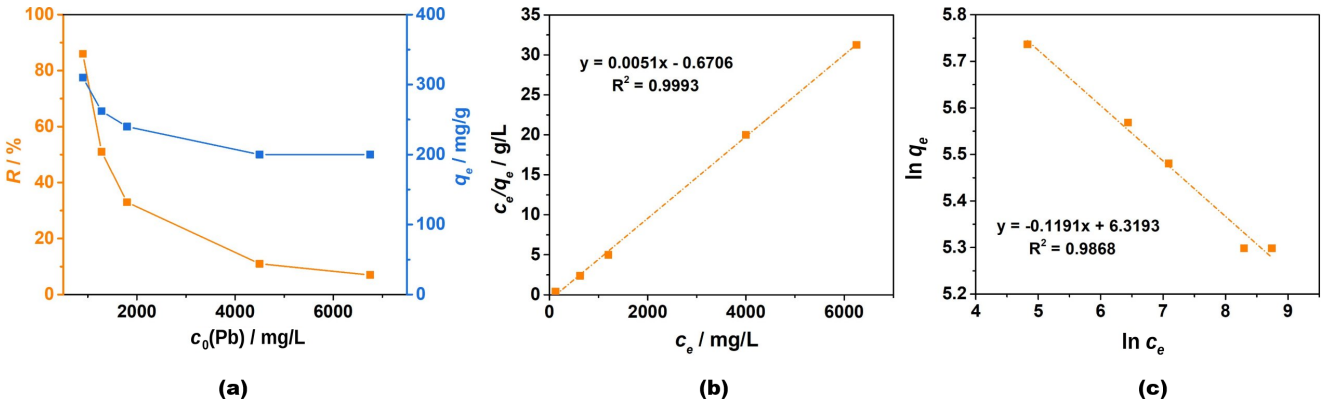


Fig. 2 Lead(II) adsorption on limestone: (a) removal efficiency and adsorption capacity as a function of the initial lead(II) concentration; (b) linear Langmuir isotherm (Eq. (3)); (c) linear Freundlich isotherm (Eq. (5)) (0.1 g limestone, 40 mL, pH 5, t = 15 min; mean values of three replicates; standard deviations are smaller than the symbol size)

variation in equilibrium concentrations for reliable isotherm modelling. Therefore, higher initial concentrations were intentionally used to achieve partial saturation of the adsorption sites and to obtain a wider equilibrium concentration range suitable for isotherm analysis. The adsorption isotherm data are presented in Table A2 (Appendix A).

Although both Langmuir and Freundlich isotherms show high coefficient of determination (R^2) (Fig. 2 (b) and (c), Table 1), the obtained parameters indicate that neither model can adequately describe Pb(II) removal under the applied concentration ($1/n < 0$, Table 1), corresponding to a physically meaningless adsorption intensity, while the Langmuir linearization displays a negative intercept, leading to negative values of K_L and R_L. Therefore, despite good linear correlations, these parameters cannot be interpreted within the assumptions of the classical Langmuir and Freundlich models. Recently, Ekpo et al. [40] have reported similar observations and emphasized that model applicability should not be judged exclusively by the regression coefficient, but also by the physical significance of the obtained parameters. Here, the limited applicability of classical isotherm models under the investigated conditions is consistent with the mechanistic examination presented in Section 3.3, which demonstrates that Pb(II) removal proceeds through a sequence of coupled processes, including calcite dissolution, ion exchange and formation of Pb-containing carbonate phases, rather than through a single equilibrium adsorption mechanism. For comparison purposes, the apparent Langmuir adsorption capacity obtained from the linearized model (q_{max} = 196 mg/g, Table 1) was comparable to the value reported by Alkhatib et al. [13] for pure calcite (Roth, $CaCO_3$ > 99%, Art.-No. P012.2), which exhibited an adsorption capacity of 156 mg/g. The obtained value was higher than those reported for different natural calcite-based materials, including natural calcite from Hungary investigated by Németh et al. [41] with an adsorption capacity of 3.1 mg/g, calcite-containing soil from Mexico studied by Rangel-Porras et al. [42] with 40 mg/g, and limestone from the field of Al-Quds University reported by Alkhatib et al. [13] with 75 mg/g.

3.2 Adsorption kinetics

The results of the kinetic study of lead ion adsorption on calcite and graphical representations of experimental data are presented in Appendix A (Table A3, Fig. A2). The experimental data were analyzed using the pseudo-first-order (PFO) and pseudo-second-order (PSO) kinetic models (Fig. A1, Appendix A) to describe the adsorption rate and identify the dominant rate-controlling processes during Pb^{2+} removal. Kinetic modelling provides valuable information on the adsorption mechanism and allows comparison of the experimental behaviour with commonly accepted adsorption models.

Overall, the PSO model showed better agreement with the experimental data than the PFO model, as indicated by the higher coefficient of determination (Table 1), which is consistent with previous studies of Pb^{2+} adsorption onto calcite and carbonate-based adsorbents [43]. The better fit of the PSO model suggests that the adsorption rate is predominantly controlled by surface interactions occurring during Pb^{2+} uptake.

A more detailed analysis reveals dual kinetic behaviour during lead removal. The first three experimental points in the initial stage (t < 15 min) are in better agreement with the pseudo-first-order (PFO) trend compared to the overall pseudo-second-order (PSO) linearisation, suggesting that the removal process cannot be well described by

a single kinetic model throughout the whole adsorption period. This indicates that quick surface reactions occur shortly after the interaction of Pb^{2+} ions with the limestone surface, probably with a change of the surface characteristics due to the partial dissolution of calcite. For contact times higher than 15 min, the experimental data are in good agreement with the PSO model, indicating the gradual dominance of chemically controlled surface processes on the uptake rate [44]. The transition between these two kinetic stages suggests that Pb^{2+} removal is governed by several coupled processes rather than a single rate-controlling mechanism, including rapid surface interaction followed by slower surface reactions such as ion exchange and/or surface complexation [45, 46].

Godelitsas et al. [47], studying lead sorption on calcite, concluded that at lower initial concentrations (10 mg/L), the adsorption process is completed within 1 min, and within 10 min at an initial concentration of 100 mg/L. At an initial concentration of 1000 mg/L, which is on the same order of magnitude as in this study, they reported that the practical end of the adsorption process occurs at 90 min, by which point more than 90% of lead was adsorbed in our experiments.

This interpretation is further supported by the time-resolved FTIR and XRD analyses presented in Section 3.3, which indicate progressive changes in the calcite surface and the formation of new Pb-containing phases during the adsorption process.

3.3 Mechanistic study of lead(II) adsorption on natural limestone

3.3.1 Structural characterization of the limestone material before and after contact with lead(II) ions

To gain insight into the mechanism of Pb(II) removal by natural limestone, the sorbent was first characterized before and after treatment with Pb^{2+}-ion containing solution using FTIR-ATR and XRD analyses.

FTIR spectra of limestone before and after Pb(II) treatment are presented in Fig. 3 (a). The pristine sample showed typical vibrations of calcite ($CaCO_3$) visible as three main distinctive bands at 1402, 873, and 713 cm^{-1}. These bands correspond to asymmetric (v_3 and v_2) and symmetric (v_4) CO_3^{2-} deformation in calcite, respectively Fathy et al. [48] and Wang et al. [49]). Weak band occurring at 1796 cm^{-1} is attributed to CO_3^{2-} $v_1 + v_4$ deformation mode, while the band at 2511 cm^{-1} relates to $2v_2 + v_4$ CO_3^{2-} deformation [50, 51]. The small band at 424 cm^{-1} is assigned to the Ca–O symmetric vibration [48]. In addition to the typical $CaCO_3$ bands, the FTIR spectrum of limestone also reveals a small amount of quartz (SiO_2) in the sample. A small band at about 1100 cm^{-1} is characteristic of Si–O–Si asymmetric stretching in quartz, while Si–O–Si out-of-plane deformations are visible at 470 cm^{-1} [52]. The corresponding XRD pattern of natural limestone powder revealed its high crystallinity (Fig. 3 (b)), which proved advantageous for Pb^{2+} ion immobilization. The observed

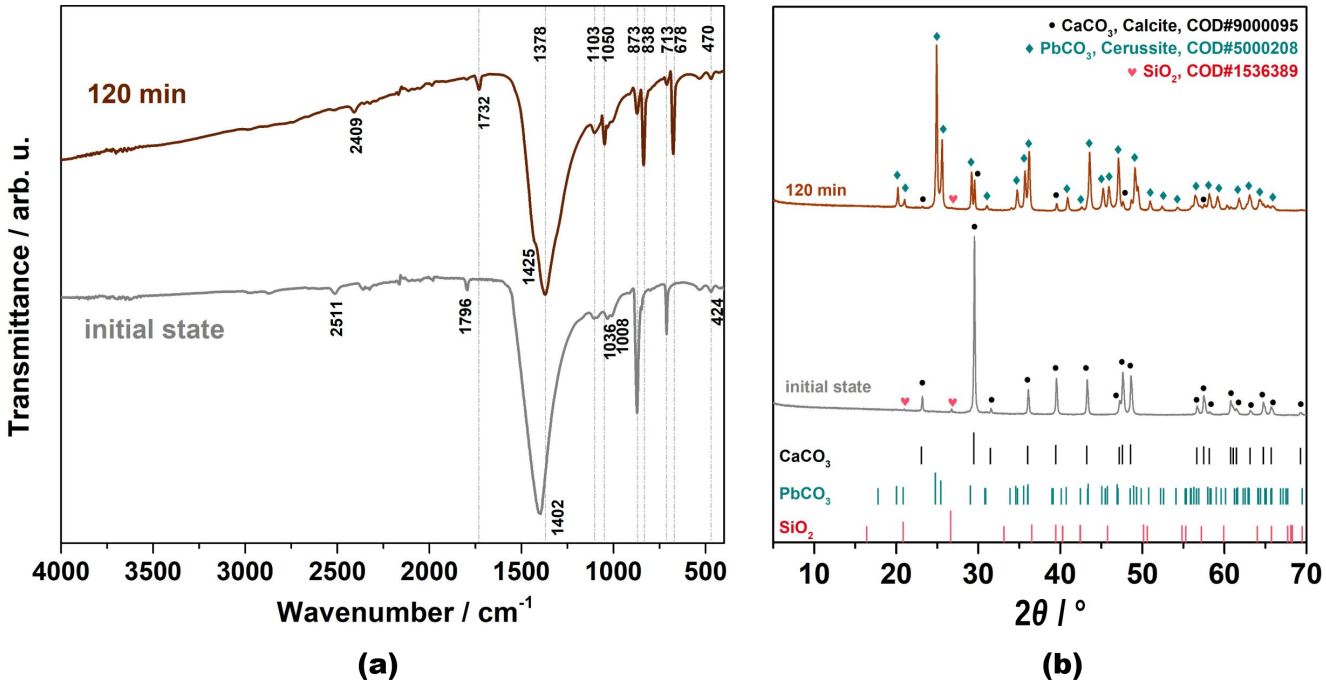


Fig. 3 Natural limestone before (0 min) and after lead(II) adsorption (120 min): (a) FTIR-ATR spectra; (b) X-ray diffractograms

reflections mainly indicate the calcite phase, accompanied by a smaller amount of quartz. Sharp reflections at 2θ angles: 29.56°, 36.12°, 39.57°, 43.29°, 47.65°, and 48.60°, match well with COD#9000095 for the trigonal calcite phase. The strongest reflection at 29.56° 2θ indicates that natural limestone mainly consists of $CaCO_3$, primarily grown along the (104) plane. Two weaker peaks at 2θ positions of 20.96° and 26.76° correspond to the most prominent SiO_2 reflections, according to COD#1536389.

Following Pb(II) removal, the FTIR spectrum showed several major changes. Calcite bands at 873 and 713 cm^{-1} significantly weaken, while new bands characteristic of cerussite ($PbCO_3$) emerge at 1050, 838, and 678 cm^{-1}. The band at 1050 cm^{-1} is ascribed to C–O symmetric vibration, while typical cerussite bands occur at 838 and 678 cm^{-1}. As for calcite, they relate to v_2 out-of-plane bending and v_4 in-plane bending of the carbonate ion, respectively, both red-shifted due to changes in crystal structure, which may be caused by the exchange of a Ca-ion with a large Pb-ion [53]. Additionally, the main broad band of calcite (1402 cm^{-1}) shifts slightly to 1378 cm^{-1}, and a new shoulder at 1425 cm^{-1} appears, indicating changes in the local carbonate environment associated with Pb incorporation. The bands related to SiO_2 are still visible after adsorption. These observations are consistent with the XRD results, where new strong reflections assigned to cerussite appear after Pb(II) treatment, while calcite diffraction lines also remain clearly visible. The main reflections at 2θ positions: 20.19°, 21.00°, 24.89°, 25.58°, 29.17°, 36.18°, 43.59°, 47.08°, and 49.10° correspond to $PbCO_3$, COD#5000208. The perseverance of calcite reflections indicates that only a fraction of the surface undergoes transformation and that the reaction is largely limited to the outer surface of the limestone particles.

Overall, the structural characterisation before and after Pb(II) treatment confirms that the removal process is associated with structural changes of the sorbent. To further describe the time evolution of these transformations and to relate them to the adsorption kinetics, *ex-situ* FTIR and XRD analyses were then carried out at different contact times.

3.3.2 Correlation between adsorption kinetics and structural evolution of the sorbent

Since the kinetic analysis revealed a clear transition between the initial (<15 min) and later adsorption stages (see Section 3.2), *ex-situ* FTIR and XRD analyses (Fig. 4) were performed to determine whether these kinetic changes correspond to structural evolution of the sorbent during Pb(II) removal.

During the first minutes of contact, the XRD patterns show only weak reflections corresponding to cerussite, while the calcite reflections remain practically unchanged (Fig. 4 (a)). Similarly, FTIR spectra reveal only weak $PbCO_3$ bands at approximately 838 and 678 cm^{-1}, whereas the characteristic calcite vibrations remain dominant (Fig. 4 (b)). These observations indicate that only limited cerussite formation occurs during the earliest stage of the process. Interestingly, the weak quartz reflection at $2\theta \approx 26.76°$ (marked with blue line at Fig. 4 (a)) temporarily disappears during the initial stage of adsorption and reappears after approximately 30 min. In contrast, the characteristic Si–O–Si vibration near 1100 cm^{-1} remains visible throughout the entire treatment. This suggests that SiO_2 molecules present on the limestone surface may initially serve as active sites for Pb^{2+} ions, especially in an acidic environment, where the surface is partially protonated [54]. Under our conditions, at pH = 5, Pb^{2+} may electrostatically interact with silanol groups, without disrupting the Si–O–Si network. Bearing in mind that this is a complex, heterogeneous system in which $CaCO_3$ partially dissolves under acidic conditions, Pb^{2+} ions, electrostatically bound to silanol groups or near the limestone surface, are prone to react initially with dissolved CO_3^{2-} ions. Consequently, the temporary disappearance of the quartz reflection in XRD is more likely related to surface coverage and microstructural effects than to dissolution of SiO_2. This behaviour is consistent with the kinetic analysis, where the initial stage deviates from the pseudo-second-order model and is better described by rapid electrostatic interactions and the onset of surface reactions.

As the contact time increases, both FTIR and XRD demonstrate the progressive growth of the cerussite phase. The appearance of the third characteristic cerussite band at approximately 1050 cm^{-1}, together with the gradual increase in cerussite reflections and the corresponding decrease in calcite reflections, indicates continuous conversion of surface carbonate species into $PbCO_3$. This is quantified using the relative intensity ratio of the two most intense reflections of cerussite and calcite ($I(2\theta) \approx 24°$ and $I(2\theta) \approx 29°$, respectively), as summarized in Appendix A Table A4. Up to 15 min, cerussite formation proceeds only to a limited extent, i.e., in the initial stage of the process. Within this time range (after 10 min of the treatment) the principal calcite band at about 1402 cm^{-1} shifts to lower wavenumbers, suggesting gradual modification of the carbonate environment accompanying Pb incorporation and probably Ca-Pb exchange. After 15 min, the progressive

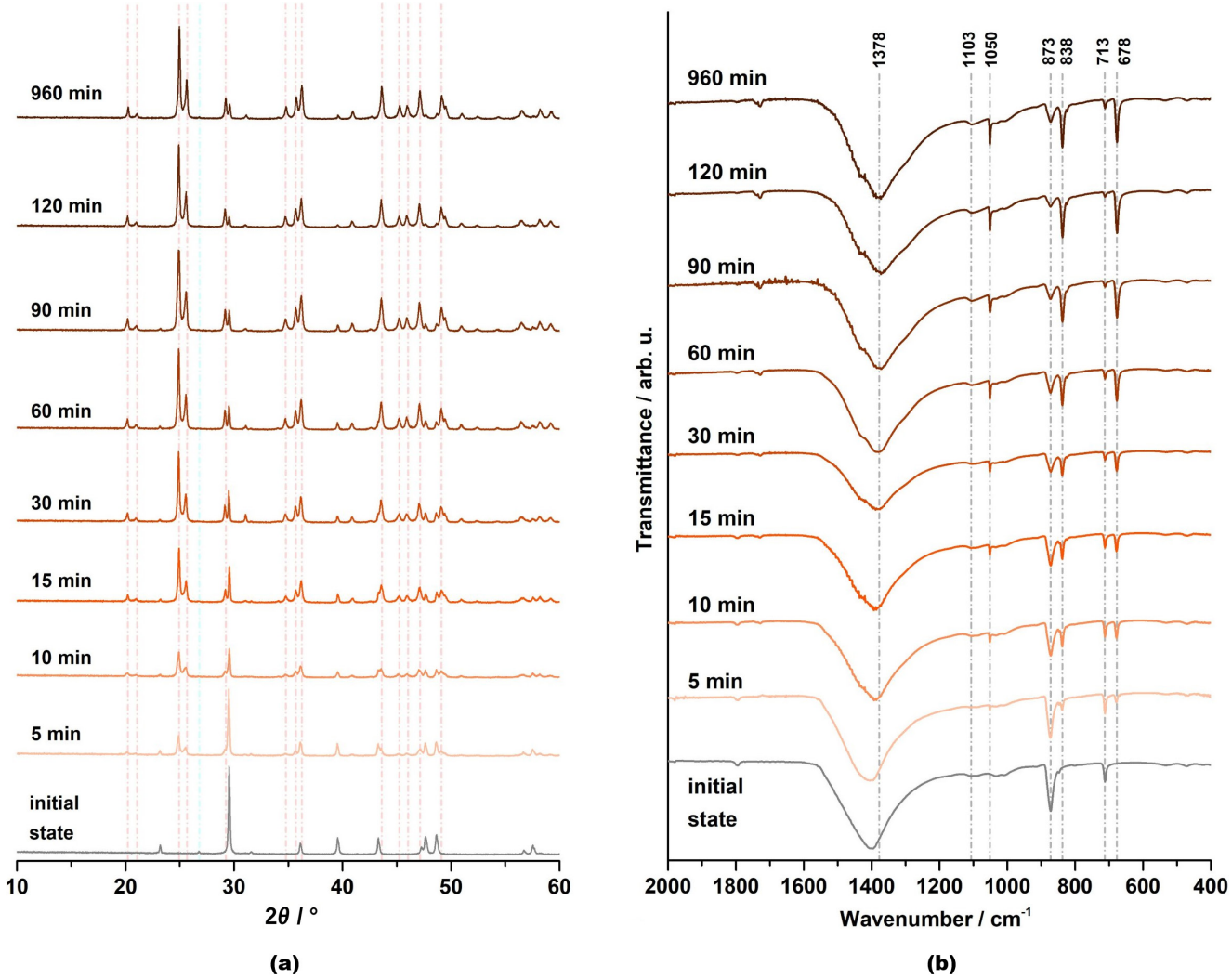


Fig. 4 *Ex-situ* characterization of natural limestone at different lead(II) adsorption times (0–960 min): (a) X-ray diffractograms; (b) FTIR-ATR spectra

increase in cerussite reflections, together with the continuous shift and intensity changes of the carbonate vibrations, indicates the establishment of sustained ion exchange accompanied by continuous cerussite nucleation and growth. This structural evolution coincides with the transition to pseudo-second-order kinetic behaviour (Fig. A1, Appendix A), suggesting that chemically controlled processes become increasingly important as the reaction proceeds. Consequently, Pb(II) removal is best described as a time-dependent, coupled mechanism involving initial electrostatic interaction, partial calcite dissolution, progressive ion exchange and surface precipitation of cerussite until equilibrium is reached.

3.4 Influence of competing ions

Wastewater and natural waters usually contain several dissolved metal ions that may interact with each other and compete for adsorption sites. Therefore, evaluation of competitive effects is essential for assessing the applicability of calcite-rich limestone material in complex aqueous systems. The extent of competition depends on several factors, including ionic charge, ionic radius, hydrated ionic radius, electronegativity, and concentration of competing species [55].

The influence of competing ions on Pb^{2+} adsorption was investigated in binary systems containing Pb^{2+} and Ni^{2+}, Cd^{2+}, Cu^{2+}, Cr^{3+}, Zn^{2+}, Mn^{2+}, Fe^{3+}, Al^{3+} and As^{3+}. The results are presented in Fig. 5 (a). The Pb^{2+} removal efficiency in the absence of competing ions was 58.8%, which was used as a reference value.

The presence of different competing ions resulted in variable effects on Pb^{2+} adsorption, including inhibitory and slightly promoting effects. The strongest inhibition was observed in the presence of Cr^{3+}, where Pb^{2+} removal decreased to 0%, indicating a pronounced negative effect of this ion on lead ions uptake. Significant decreases were also observed for Al^{3+} (15%) and Cu^{2+} (34%), suggesting strong competition between these ions and Pb^{2+} for available adsorption sites.

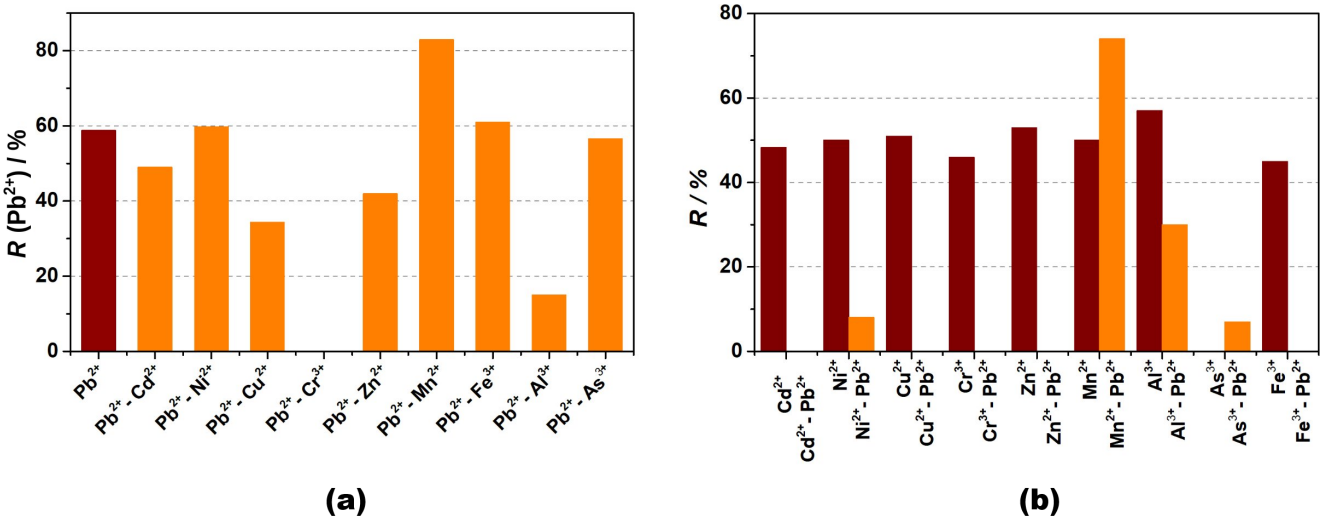


Fig. 5 Removal efficiency in binary systems: (a) effect of competing cations on lead(II) removal by limestone; (b) effect of lead(II) on the removal of the competing metals

Moderate inhibition was observed for Cd^{2+} (49%), Zn^{2+} (42%), and As^{3+} (57%), while Ni^{2+} showed almost no influence on lead removal (60%), indicating that this ion does not significantly interfere with Pb^{2+} adsorption under the investigated conditions. In contrast, the presence of Mn^{2+} (83%) and Fe^{3+} (61%) slightly enhanced lead removal compared with the single-metal system. This behavior may be associated with changes in the surface chemistry or solution conditions caused by these ions; however, additional analyses would be required to confirm the exact mechanism.

The reverse effect, namely the influence of Pb^{2+} on the adsorption of other metals, is shown in Fig. 5 (b). The presence of Pb^{2+} generally suppressed the adsorption of competing ions, confirming the high affinity of Pb^{2+} toward limestone surface sites. Complete inhibition was observed for Cd^{2+}, Cu^{2+}, Cr^{3+}, Zn^{2+}, and Fe^{3+}, while adsorption of Ni^{2+} decreased from 50% to 8.1% and Al^{3+} from 57% to 30%.

An exception was observed for Mn^{2+}, whose adsorption increased from 50% in the single-metal system to 74% in the presence of Pb^{2+}. Although direct evidence of synergistic Mn^{2+} adsorption in the presence of Pb^{2+} is limited, similar effects have been associated with changes in surface reactions and the formation of additional adsorption sites in mineral systems containing Mn phases [56, 57].

For As^{3+}, which showed negligible adsorption on calcite under the studied conditions, the presence of Pb^{2+} resulted in a small removal efficiency (7.0%). This behavior may indicate secondary processes such as co-precipitation or the formation of mixed interfacial phases rather than direct competitive adsorption.

Overall, these results demonstrate that Pb^{2+} adsorption on limestone is affected by the presence of other metal ions, highlighting the importance of evaluating competitive interactions when applying adsorbents for treatment of complex contaminated waters.

3.5 Desorption studies

The ability to remove lead ions from the surface of limestone is of considerable environmental importance due to the high toxicity and persistence of lead in the environment. Desorption in deionized water and rainwater was negligible (0.01% and 0.05%, respectively), indicating that Pb^{2+}-saturated limestone is stable under typical environmental conditions and does not pose an immediate contamination risk. In contrast, desorption in EDTA solutions was significantly higher: 58% Pb^{2+} was removed with 0.0025 M EDTA, while 0.01 M EDTA led to almost complete desorption. This trend reflects the strong affinity of EDTA toward Pb^{2+} and its ability to promote lead release from the solid phase. Namely, EDTA is a chelating agent that forms an exceptionally stable complex with Pb^{2+} ($\log K \approx 18$), with the chelate effect further enhancing this stability. By removing free Pb^{2+} ions from solution, EDTA shifts the dissolution equilibrium of sparingly soluble $PbCO_3$ toward greater lead release, thereby effectively increasing the solubility of this salt. This effect is stronger at higher EDTA concentrations, because more ligand is available to bind the Pb^{2+} released from the solid phase [58, 59]. Lead-containing EDTA solutions generated during the desorption process require further treatment before discharge due to the high stability of Pb–EDTA complexes. Previous studies have shown that lead can be recovered from Pb–EDTA solutions using electrochemical treatment with a graphite anode, while photochemical and chemical oxidation processes can promote EDTA degradation and facilitate further treatment of the

released lead species [60]. Therefore, although EDTA is effective for regenerating Pb-loaded limestone, the resulting Pb–EDTA solutions should be considered as secondary waste streams requiring appropriate management.

3.6 Lead(II) removal in real systems

Previous experiments demonstrated that limestone material can effectively remove Pb^{2+} from aqueous solutions. Based on these findings, the performance of limestone was further evaluated using real surface water affected by acidic mine drainage.

Experiments were performed using stream water samples collected from the Šuplja Stijena mine site, Pljevlja, Montenegro. The batch experiments were conducted according to the procedure described in Section 2.2.5.

The batch treatment of Mjedenički stream water demonstrated that limestone significantly reduced Pb concentrations under natural pH conditions. The initial dissolved Pb concentrations ranged from 208 to 708 μg/L, while final concentrations were reduced to 23–36 μg/L (Table 2). These results indicate effective Pb removal from mine-impacted water under the investigated conditions.

The observed removal efficiency was achieved using a relatively small amount of limestone (1 g in batch experiments). These findings indicate the potential of limestone as a low-cost material for Pb removal from mine-affected waters, although further long-term studies are required before field-scale application. The flow-through experiments provide preliminary evidence of limestone performance under continuous-flow conditions. However, these results should be interpreted with caution, as laboratory-scale removal efficiency alone does not provide a complete assessment of environmental suitability. Long-term studies, including continuous-flow breakthrough experiments and comprehensive water quality monitoring, are required to evaluate the stability and practical applicability of the treatment process.

In the flow system, experiments were performed at a constant flow rate of 200 L/h and initial Pb concentration of 208 μg/L, the fine fraction achieved the fastest pH increase to 6.0 within 45 min, followed by the medium (60 min) and coarse (165 min) fractions. Correspondingly, lead removal efficiency improved with decreasing particle size, with final concentrations of 98 μg/L (coarse), 17.8 μg/L (medium), and 8.72 μg/L (fine). These findings are consistent with the influence of particle size observed in experiments with model solutions, highlighting the higher reactivity of finer limestone fractions, likely related to their greater available surface area.

Table 2 Lead removal from Mjedenički stream water under batch conditions

Year	Pb initial concentration [μg/L]	Pb final concentration [μg/L]	R [%]
2023	708 ± 47	23.3 ± 1.5	96.7
2024	208 ± 14	36.7 ± 2.4	82.7
2025	470 ± 31	27.4 ± 1.8	94.3

The residual Pb concentration obtained using the fine fraction was below the reported Maximum Allowable Concentration – Environmental Quality Standard (MAC-EQS) value for surface waters according to the Montenegrin regulation aligned with the EU Water Framework Directive [24, 61, 62]. This comparison indicates that the treated water achieved a Pb concentration lower than the regulatory threshold under the tested laboratory flow conditions; however, long-term compliance would require additional validation through extended operation and monitoring.

The results demonstrated the high Pb removal efficiency of calcite-rich limestone material, even at low pH and in the presence of multiple competing metal ions. For comparison, Mzinyane [63] reported over 99% Pb^{2+} removal from acid mine drainage within 20 min using poly(hydroxamic acid) ligands, while An et al. [64] achieved 87.6–91.4% Pb^{2+} removal using an oyster shell–lignite composite. Kragović [65] showed that natural zeolite reduced Pb^{2+} concentration from 0.333 mg/L to 0.009 mg/L, while Fe(III)-modified zeolite achieved complete Pb^{2+} removal.

4 Conclusions

This study investigated the applicability of natural calcite-rich limestone from the Šuplja Stijena mine area as a low-cost material for Pb(II) removal from synthetic solutions and real mining-impacted waters. Removal efficiency under different experimental conditions was examined, while kinetic modelling together with FTIR and XRD analyses provided insight into the mechanisms governing Pb(II) immobilization.

The Pb^{2+} removal process was rapid and followed pseudo-second-order kinetics over the overall adsorption period, while deviations during the initial stage indicate the coexistence of several coupled processes. The equilibrium data could not be satisfactorily interpreted using classical Langmuir or Freundlich adsorption models. This finding is consistent with the mechanistic evidence obtained from kinetic, FTIR, and XRD analyses, which indicates that Pb(II) removal proceeds through calcite dissolution, ion exchange, surface interactions, and

progressive cerussite formation rather than by a single equilibrium adsorption mechanism. The presence of competing ions affected Pb removal efficiency, with Cr^{3+}, Cu^{2+}, and Al^{3+} showing the strongest inhibitory effects.

Desorption experiments showed that Pb bound to calcite is highly stable in deionized water and rainwater, while EDTA promoted significant Pb release from the solid phase. These findings indicate the potential for chemical regeneration of Pb-loaded calcite; however, repeated regeneration cycles and the long-term stability of regenerated material require further evaluation.

The performance of calcite-rich limestone in real mine-impacted water demonstrated its potential applicability for Pb removal under laboratory batch and flow-through conditions. Nevertheless, detailed long-term experiments, comprehensive water quality assessment, and further evaluation of material regeneration are required before practical field-scale application can be fully established. In addition, a more detailed understanding of the coupled Pb–calcite interaction mechanisms and the fate of Pb-loaded limestone would further support the optimization and sustainable application of this material.

References

[1] Nasser, N., El-Sayed, M. I., Othman, S. I., Allam, A. A., Al-Labadi, I. G., Abukhadra, M. R., Bellucci, S. "Systematic Evaluation for the Impact of the Geological Conditions on the Adsorption Affinities of Calcite as an Adsorbent of Zn^{2+} Ions from Aqueous Solutions: Experimental and Theoretical Studies", Minerals, 12(12), 1635, 2022. https://doi.org/10.3390/min12121635

[2] Sayed, I. R., Farhan, A. M., AlHammadi, A. A., El-Sayed, M. I., Abd El-Gaied, I. M., El-Sherbeeny, A. M., Al Zoubi, W., Ko, Y. G., Abukhadra, M. R. "Synthesis of novel nanoporous zinc phosphate/hydroxyapatite nano-rods (ZPh/HPA_{NRs}) core/shell for enhanced adsorption of Ni^{2+} and Co^{2+} ions: Characterization and application", Journal of Molecular Liquids, 360, 119527, 2022. https://doi.org/10.1016/j.molliq.2022.119527

[3] Chen, Y., Nie, Z., Gao, J., Wang, J., Cai, M. "A novel adsorbent of bentonite modified chitosan-microcrystalline cellulose aerogel prepared by bidirectional regeneration strategy for Pb(II) removal", Journal of Environmental Chemical Engineering, 9(4), 105755, 2021. https://doi.org/10.1016/j.jece.2021.105755

[4] Kadeche, A., Ramdani, A., Adjdir, M., Guendouzi, A., Taleb, S., Kaid, M., Deratani, A. "Preparation, characterization and application of Fe-pillared bentonite to the removal of Coomassie blue dye from aqueous solutions", Research on Chemical Intermediates, 46(11), pp. 4985–5008, 2020. https://doi.org/10.1007/s11164-020-04236-2

[5] Bulgariu, L., Ferţu, D. I., Cara, I. G., Gavrilescu, M. "Efficacy of Alkaline-Treated Soy Waste Biomass for the Removal of Heavy-Metal Ions and Opportunities for Their Recovery", Materials, 14(23), 7413, 2021. https://doi.org/10.3390/ma14237413

[6] Azanfire, B.-E., Bulgariu, D., Cimpoeşu, N., Bulgariu, L. "Efficient Removal of Toxic Heavy Metals on Kaolinite-Based Clay: Adsorption Characteristics, Mechanism and Applicability Perspectives", Water, 17(13), 1938, 2025. https://doi.org/10.3390/w17131938

[7] Sabry, M., Alazab, H. A., Gad, A., El-Faramawy, N. "Thermoluminescence properties of natural Egyptian calcite", Journal of Luminescence, 238, 118273, 2021. https://doi.org/10.1016/j.jlumin.2021.118273

[8] Tangarfa, M., Semlali Aouragh Hassani, N., Alaoui, A. "Behavior and Mechanism of Tannic Acid Adsorption on the Calcite Surface: Isothermal, Kinetic, and Thermodynamic Studies", ACS Omega, 4(22), pp. 19647–19654, 2019. https://doi.org/10.1021/acsomega.9b02259

[9] Carchini, G., Hussein, I., Al-Marri, M. J., Shawabkeh, R., Mahmoud, M., Aparicio, S. "A theoretical study of gas adsorption on calcite for CO_2 enhanced natural gas recovery", Applied Surface Science, 504, 144575, 2020. https://doi.org/10.1016/j.apsusc.2019.144575

[10] Wang, J., Zhao, J., Qiao, Y., Luan, Z. "Effect of Mg(II), Mn(II), and Fe(II) doping on the mechanical properties and electronic structure of calcite", Materials Today Communications, 31, 103725, 2022. https://doi.org/10.1016/j.mtcomm.2022.103725

[11] Gunasekaran, S., Anbalagan, G. "Spectroscopic characterization of natural calcite minerals", Spectrochimica Acta Part A: Molecular and Biomolecular Spectroscopy, 68(3), pp. 656–664, 2007. https://doi.org/10.1016/j.saa.2006.12.043

[12] Fiorito, E., Porcedda, G. E., Brundu, L., Passiu, C., Atzei, D., Ennas, G., Elsener, B., Fantauzzi, M., Rossi, A. "Calcium carbonate as sorbent for lead removal from wastewaters", Chemosphere, 296, 133897, 2022. https://doi.org/10.1016/j.chemosphere.2022.133897

[13] Alkhatib, M., Ayyad, O., Tbakhi, R., Qurie, M. "A comparative study for lead removal by pure calcite and a natural calcitic soil sample", International Journal of Environmental Science and Technology, 20(11), pp. 12243–12250, 2023. https://doi.org/10.1007/s13762-023-04826-8

[14] Shref, A. M., Al Maamouri, A. B. D. S., Khudhair, M. F., Ahmed, F. W. "Effect of clay minerals, calcite, and organic matter on adsorption and desorption of cadmium and lead", Iraqi Journal of Agricultural Sciences, 55(5), pp. 1657–1666, 2024. https://doi.org/10.36103/zfgk8x49

[15] ISME "MEST EN ISO 5667-1:2023 Kvalitet vode - Uzimanje uzoraka - Dio 1: Uputstvo za izradu programa uzimanja uzoraka i tehnike uzimanja uzoraka" (MEST EN ISO 5667-1:2023 Water quality - Sampling - Part 1: Guidance on the design of sampling programmes and sampling techniques), Institute for Standardization of Montenegro (ISME), Podgorica, Montenegro, 2023. (in Montenegrin)

[16] ISME "MEST EN ISO 5667-6:2017 Kvalitet vode - Uzorkovanje - Dio 6: Uputstvo za uzorkovanje iz rijeka i potoka" (MEST EN ISO 5667-6:2017 Water quality - Sampling - Part 6: Guidance on sampling of rivers and streams), Institute for Standardization of Montenegro (ISME), Podgorica, Montenegro, 2017. (in Montenegrin)

[17] ISO "ISO 11885:2007 Water quality — Determination of selected elements by inductively coupled plasma optical emission spectrometry (ICP-OES)", International Organization for Standardization, Geneva, Switzerland, 2007.

[18] Liu, M., Zou, D., Ma, T., Liu, Z., Li, Y. "Simultaneous efficient adsorption and accelerated photocatalytic degradation of chlortetracycline hydrochloride over novel Fe-based MOGs under visible light irradiation assisted by hydrogen peroxide", Inorganic Chemistry Frontiers, 6(6), pp. 1388–1397, 2019. https://doi.org/10.1039/c9qi00046a

[19] Langmuir, I. "The adsorption of gases on plane surfaces of glass, mica and platinum", Journal of the American Chemical Society, 40(9), pp. 1361–1403, 1918. https://doi.org/10.1021/ja02242a004

[20] Hall, K. R., Eagleton, L. C., Acrivos, A., Vermeulen, T. "Pore- and Solid-Diffusion Kinetics in Fixed-Bed Adsorption under Constant-Pattern Conditions", Industrial & Engineering Chemistry Fundamentals, 5(2), pp. 212–223, 1966. https://doi.org/10.1021/i160018a011

[21] Freundlich, H. M. F. "Über die Adsorption in Lösungen" (On adsorption in solutions), Zeitschrift für Physikalische Chemie, 57U(1), pp. 385–470, 1907. (in German) https://doi.org/10.1515/zpch-1907-5723

[22] Lagergren, S. "Zur Theorie der sogenannten Adsorption gelöster Stoffe" (About the theory of so-called adsorption of soluble substances), Kungliga Svenska Vetenskapsakademiens Handlingar, 24(4), pp. 1–39, 1898. (in German)

[23] Ho, Y. S., McKay, G. "Pseudo-second order model for sorption processes", Process Biochemistry, 34(5), pp. 451–465, 1999. https://doi.org/10.1016/S0032-9592(98)00112-5

[24] Vlada Crne Gore "No. 25/19, Pravilnik o načinu i rokovima utvrđivanja statusa površinskih voda" (No. 25/19 Rulebook on the manner and deadlines for determining the status of surface waters), Podgorica, Montenegro, 2019. [online] Available at: https://www.gov.me/dokumenta/e0293a19-d141-48fd-b03d-80a3333190ee [Accessed: 05 August 2026] (in Montenegrin)

[25] Bidhendi, M. E., Gabris, M. A., Goudarzi, V., Abedynia, S., Juma, B. H., Sereshti, H., Kamboh, M. A., Soylak, M., Nodeh, H. R. "Removal of some heavy metal ions from water using novel adsorbent based on iron oxide-doped sol-gel organic-inorganic hybrid nanocomposite: equilibrium and kinetic studies", Desalination and Water Treatment, 147, pp. 173–182, 2019. https://doi.org/10.5004/dwt.2019.23482

[26] Çelebi, H., Gök, G., Gök, O. "Adsorption capability of brewed tea waste in waters containing toxic lead(II), cadmium (II), nickel (II), and zinc(II) heavy metal ions", Scientific Reports, 10(1), 17570, 2020. https://doi.org/10.1038/s41598-020-74553-4

[27] Ali, R. M., Hamad, H. A., Hussein, M. M., Malash, G. F. "Potential of using green adsorbent of heavy metal removal from aqueous solutions: Adsorption kinetics, isotherm, thermodynamic, mechanism and economic analysis", Ecological Engineering, 91, pp. 317–332, 2016. https://doi.org/10.1016/j.ecoleng.2016.03.015

[28] Fadhel Ali, F., Al-Rawi. A. S., Aljumialy, A. M. "Limestone residues of sculpting factories utilization as sorbent for removing Pb(II) ion from aqueous solution", Results in Chemistry, 4, 100621, 2022. https://doi.org/10.1016/j.rechem.2022.100621

[29] Kostić, M. M. "Sinteza i karakterizacija ksantovanih biosorbenata i njihova primena za uklanjanje katjonskih polutanata iz vodenih rastvora" (Synthesis and characterization of xanthated biosorbents and their application for the removal of cationic pollutants from aqueous solutions), PhD thesis, University of Niš, , 2014. [online] Available at: https://www.pmf.ni.ac.rs/download/doktorati/dokumenta/disertacije/2014/2014-09-25-km.pdf [Accessed: 05 August 2026] (in Serbian)

[30] Feng, N., Guo, X., Liang, S. "Kinetic and thermodynamic studies on biosorption of Cu(II) by chemically modified orange peel", Transactions of Nonferrous Metals Society of China, 19(5), pp. 1365–1370, 2009. https://doi.org/10.1016/S1003-6326(08)60451-3

[31] Feng, N., Guo, X., Liang, S., Zhu, Y., Liu, J. "Biosorption of heavy metals from aqueous solutions by chemically modified orange peel", Journal of Hazardous Materials, 185(1), pp. 49–54, 2011. https://doi.org/10.1016/j.jhazmat.2010.08.114

[32] Homagai, P. L., Ghimire, K. N., Inoue, K. "Adsorption behavior of heavy metals onto chemically modified sugarcane bagasse", Bioresource Technology, 101(6), pp. 2067–2069, 2010. https://doi.org/10.1016/j.biortech.2009.11.073

[33] Ibrahim, H. S., Ammar, N. S., Soylak, M., Ibrahim, M. "Removal of Cd(II) and Pb(II) from aqueous solution using dried water hyacinth as a biosorbent", Spectrochimica Acta Part A: Molecular and Biomolecular Spectroscopy, 96, pp. 413–420, 2012. https://doi.org/10.1016/j.saa.2012.05.039

[34] Gong, R., Ding, Y., Liu, H., Chen, Q., Liu, Z. "Lead biosorption and desorption by intact and pretreated *spirulina maxima* biomass", Chemosphere, 58(1), pp. 125–130, 2005. https://doi.org/10.1016/j.chemosphere.2004.08.055

[35] Hossain, M. A., Hao Ngo, H., Guo, W. S., Nguyen, T. V. "Removal of Copper from Water by Adsorption onto Banana Peel as Bioadsorbent", International Journal of GEOMATE, 2(4), pp. 227–234, 2012. [online] Available at: https://geomatejournal.com/geomate/article/view/1452 [Accessed: 05 August 2026]

[36] Bashyal, D., Homagai, P. L., Ghimire, K. N. "Removal of Lead from Aqueous Medium Using Xanthate Modified Apple Juice Residue", Journal of Nepal Chemical Society, 26, pp. 53–60, 2010. https://doi.org/10.3126/jncs.v26i0.3632

[37] Babel, S., Kurniawan, T. A. "Low-cost adsorbents for heavy metals uptake from contaminated water: a review", Journal of Hazardous Materials, 97(1–3), pp. 219–243, 2003. https://doi.org/10.1016/S0304-3894(02)00263-7

[38] Foo, K. Y., Hameed, B. H. "Insights into the modeling of adsorption isotherm systems", Chemical Engineering Journal, 156(1), pp. 2–10, 2010. https://doi.org/10.1016/j.cej.2009.09.013

[39] Ozdes, D., Gundogdu, A., Kemer, B., Duran, C., Senturk, H. B., Soylak, M. "Removal of Pb(II) ions from aqueous solution by a waste mud from copper mine industry: Equilibrium, kinetic and thermodynamic study", Journal of Hazardous Materials, 166(2–3), pp. 1480–1487, 2009. https://doi.org/10.1016/j.jhazmat.2008.12.073

[40] Ekpo, I. E., Onyemaobi, N. C., Udo, I. E., Okoye, I. P. "Langmuir and Freundlich Isotherms and Pseudo-Order Kinetics of Xylene Adsorption on Succinic Acid-Modified Hardwood Sawdust", Open Journal of Physical Chemistry, 16(1), pp. 25–38, 2026. https://doi.org/10.4236/ojpc.2026.161002

[41] Németh, G., Mlinárik, L., Török, Á. "Adsorption and chemical precipitation of lead and zinc from contaminated solutions in porous rocks: Possible application in environmental protection", Journal of African Earth Sciences, 122, pp. 98–106, 2016. https://doi.org/10.1016/j.jafrearsci.2016.04.022

[42] Rangel-Porras, G., García-Magno, J. B., González-Muñoz, M. P. "Lead and cadmium immobilization on calcitic limestone materials", Desalination, 262(1–3), pp. 1–10, 2010. https://doi.org/10.1016/j.desal.2010.04.043

[43] Sdiri, A., Higashi, T., Hatta, T., Jamoussi, F., Tase, N. "Removal of heavy metals from aqueous solution by limestone", International Journal of Global Environmental Issues, 12(2–4), pp. 171–178, 2012. https://doi.org/10.1504/IJGENVI.2012.049380

[44] Eddy, N. O., Garg, R., Ukpe, R. A., Ameh, P. O., Garg, R., Runde, M., Kwanchi, I. D., Wabaidur, S. M., Siddiqu, M. R., Ogbodo, R. "Application of Periwinkle Shell for the Synthesis of Calcium Oxide Nanoparticles and in the Remediation of Pb2+ Contaminated Water", [preprint] Research Square, 30 May 2023. https://doi.org/10.21203/rs.3.rs-2895593/v1

[45] Din, S. U., Arogundade, I., Al-Ahmary, K. M., Al-Mhyawi, S. R., AlMohamadi, H., Elamin, N. Y., Alshdoukhi, I. F., Alrashood, J. S. "Utilization of valorised wood bark waste as an adsorbent for the uptake of Pb(II) ions", Scientific Reports, 15(1), 31099, 2025. https://doi.org/10.1038/s41598-025-17021-1

[46] Radovanovic, D., Dikić, J., Štulović, M., Anđić, Z., Kamberović, Ž., Jevtić, S. "Sorption of Pb^{2+}, Zn^{2+}, Cu^{2+} and Ni^{2+} Ions on Na-enriched Natural Zeolite for Wastewater Treatment Process: A Kinetic Approach", Metallurgical and Materials Engineering, 29(3), pp. 20–35, 2023. https://doi.org/10.56801/mme1007

[47] Godelitsas, A., Astilleros, J. M., Hallam, K., Harissopoulos, S., Putnis, A. "Interaction of Calcium Carbonates with Lead in Aqueous Solutions", Environmental Science & Technology, 37(15), pp. 3351–3360, 2003. https://doi.org/10.1021/es020238i

[48] Fathy, A. T., Moneim, M. A., Ahmed, E. A., El-Ayaat, A. M., Dardir, F. M. "Effective removal of heavy metal ions (Pb, Cu, and Cd) from contaminated water by limestone mine wastes", Scientific Reports, 15(1), 1680, 2025. https://doi.org/10.1038/s41598-024-82861-2

[49] Wang, X., Xu, X., Ye, Y., Wang, C., Liu, D., Shi, X., Wang, S., Zhu, X. "*In-situ* High-Temperature XRD and FTIR for Calcite, Dolomite and Magnesite: Anharmonic Contribution to the Thermodynamic Properties", Journal of Earth Science, 30(5), pp. 964–976, 2019. https://doi.org/10.1007/s12583-019-1236-7

[50] Kamalanathan, P., Ramesh, S., Bang, L. T., Niakan, A., Tan, C. Y., Purbolaksono, J., Chandran, H., Teng, W. D. "Synthesis and sintering of hydroxyapatite derived from eggshells as a calcium precursor", Ceramics International, 40(10), pp. 16349–16359, 2014. https://doi.org/10.1016/j.ceramint.2014.07.074

[51] Gunasekaran, S., Anbalagan, G., Pandi, S. "Raman and infrared spectra of carbonates of calcite structure", Journal of Raman Spectroscopy, 37(9), pp. 892–899, 2006. https://doi.org/10.1002/jrs.1518

[52] Ellerbrock, R., Stein, M., Schaller, J. "Comparing amorphous silica, short-range-ordered silicates and silicic acid species by FTIR", Scientific Reports, 12(1), 11708, 2022. https://doi.org/10.1038/s41598-022-15882-4

[53] Li, X., Azimzadeh, B., Martinez, C. E., McBride, M. B. "Pb mineral precipitation in solutions of sulfate, carbonate and phosphate: Measured and modeled Pb solubility and Pb^{2+} activity", Minerals, 11(6), 620, 2021. https://doi.org/10.3390/min11060620

[54] Gamba, O. A., Badawi, M., Said, H., Barres, O., Lainé, J., Mesquita, J., Foucaud, Y. "pH-Dependent Behavior of Quartz Surfaces: Insights from XPS, DRIFT, and Potentiometric Titrations", The Journal of Physical Chemistry B, 129(37), pp. 9517–9528, 2025. https://doi.org/10.1021/acs.jpcb.5c04451

[55] Zhao, D., Zhang, Y., Wu, C. "Adsorption of Pb(II) ions by functionalized multi-walled carbon nanotubes MWCNTs-NH_2", Journal of Hazardous Materials Advances, 19, 100764, 2025. https://doi.org/10.1016/j.hazadv.2025.100764

[56] Shi, T., Jia, S., Chen, Y., Wen, Y., Du, C., Wang, Z., Qiu, R. "Adsorption Characteristics of Cu(II) and Pb(II) Ions onto Natural Manganese Ore from Aqueous Solution", Adsorption Science & Technology, 26(8), pp. 613–629, 2008. https://doi.org/10.1260/026361708788059820

[57] Tang, S.-F., Zhou, H., Tan, W.-T., Huang, J.-G., Zeng, P., Gu, J.-F., Liao, B.-H. "Adsorption Characteristics and Mechanisms of Fe-Mn Oxide Modified Biochar for Pb(II) in Wastewater", International Journal of Environmental Research and Public Health, 19(14), 8420, 2022. https://doi.org/10.3390/ijerph19148420

[58] Palden, T., MacHiels, L., Onghena, B., Regadío, M., Binnemans, K. "Selective leaching of lead from lead smelter residues using EDTA", RSC Advances, 10(69), pp. 42147–42156, 2020. https://doi.org/10.1039/d0ra08517k

[59] Kim, C., Lee, Y., Ong, S. K. "Factors affecting EDTA extraction of lead from lead-contaminated soils", Chemosphere, 51(9), pp. 845–853, 2003. https://doi.org/10.1016/S0045-6535(03)00155-3

[60] Chitra, S., Paramasivan, K., Sinha, P. K., Lai, K. B. "Treatment of Liquid Waste Containing Ethylenediamine Tetraaceticaxid by Advanced Oxidation Processes", Journal of Advanced Oxidation Technologies, 6(1), pp. 109–114, 2003. https://doi.org/10.1515/jaots-2003-0117

[61] European Parliament and the Council of the European Union, Directive 2013/39/EU of the European Parliament and of the Council of 12 August 2013 amending Directives 2000/60/EC and 2008/105/EC as regards priority substances in the field of water policy Text with EEA relevance. [online] Available at: https://eur-lex.europa.eu/eli/dir/2013/39/oj/eng [Accessed: 05 August 2026]

[62] European Parliament and the Council of the European Union, Directive 2000/60/EC of the European Parliament and of the Council of 23 October 2000 establishing a framework for Community action in the field of water policy. [online] Available at: https://eur-lex.europa.eu/eli/dir/2000/60/oj/eng [Accessed: 05 August 2026]

[63] Mzinyane, N. N. "Adsorption of heavy metals from acid mine drainage using poly (hydroxamic acid) ligand", South African Journal of Chemical Engineering, 42, pp. 318–336, 2022. https://doi.org/10.1016/j.sajce.2022.09.007

[64] An, W., Liu, Y., Chen, H., Sun, X., Wang, Q., Hu, X., Di, J. "Adsorption properties of Pb(II) and Cd(II) in acid mine drainage by oyster shell loaded lignite composite in different morphologies", Scientific Reports, 14(1), 11627, 2024. https://doi.org/10.1038/s41598-024-62506-0

[65] Kragović, M. M. "Uklanjanje jona olova iz vodenih rastvora upotrebom prirodnog i Fe(III)-modifikovanog zeolita" (Removal of lead ions from aqueous solutions by using natural and Fe(III)-modified zeolite), PhD thesis, University of Belgrade, 2014. [online] Available at: https://eteze.bg.ac.rs/application/showtheses?thesesId=3292 [Accessed: 05 August 2026] (in Serbian)

Appendix A

1 Adsorption isotherms and kinetic models

Linearized forms of the Langmuir and Freundlich isotherms and of the pseudo-first-order and pseudo-second-order kinetic models (Eqs. (3) to (7), Section 2.2.2) are summarized in Table A1.

2 Adsorption isotherm results

The results of the adsorption isotherm study of lead on limestone are presented in Table A2.

Table A1 Equations and linearized forms of the isotherm and kinetic models

Model / Parameter	Equation (linear form)	Reference
Langmuir isotherm	$\frac{c_e}{q_e} = \frac{1}{K_L q_{max}} + \frac{c_e}{q_{max}}$	[19]
Separation factor	$R_L = \frac{1}{1 + K_L c_0}$	[20]
Freundlich isotherm	$\ln q_e = \ln K_F + \frac{1}{n} \ln c_e$	[21]
Pseudo-first-order	$\ln(q_e - q_t) = \ln q_e - k_1 t$	[22]
Pseudo-second-order	$\frac{t}{q_t} = \frac{1}{k_2 q_e^2} + \frac{t}{q_e}$	[23]

c_0 and c_e (mg/L) are the initial and equilibrium concentrations of Pb(II) in solution, q_e (mg/g) is the equilibrium adsorption capacity, q_t (mg/g) is the adsorption capacity at time t (min), q_{max} (mg/g) is the maximum (monolayer) adsorption capacity, K_L (L/mg) is the Langmuir constant, R_L is the separation factor, K_F ((mg/g)(L/mg)$^{1/n}$) is the Freundlich constant, $1/n$ is the heterogeneity factor, and k_1 (1/min) and k_2 (g/(mg min)) are the PFO and PSO rate constants.

Table A2 Isotherm data for lead(II) adsorption on limestone used for the linear Langmuir (Eq. (3)) and Freundlich (Eq. (5)) models (0.1 g limestone, < 0.5 mm, 40 mL, pH 5, t = 15 min, 22 ± 2 °C)

c_0 (mg/L)	c_e (mg/L)	c_e/q_e (g/L)	ln c_e	q_e (mg/g)	ln q_e	R (%)
900 ± 59	125 ± 8	0.40	4.83	310	5.74	86.1
1280 ± 84	625 ± 41	2.39	6.44	262	5.57	51.2
1800 ± 119	1200 ± 79	5.00	7.09	240	5.48	33.3
4500 ± 297	4000 ± 264	20.0	8.29	200	5.30	11.1
6750 ± 446	6250 ± 412	31.2	8.74	200	5.30	7.41

c_0 and c_e are concentrations measured by ICP-OES and are given as mean ± expanded measurement uncertainty.

3 Adsorption kinetics results

Table A3 and Figs. A1 and A2 present the results of the kinetic study of Pb^{2+} adsorption on calcite.

4 Quantification of cerussite formation based on XRD analysis

Table A4 presents XRD-derived relative intensity ratios of cerussite and calcite reflections used to quantify surface phase transformation during Pb^{2+} adsorption.

Table A3 Kinetic data for lead(II) adsorption on limestone (c_0 = 1455 mg/L, 0.1 g limestone, < 0.5 mm, 40 mL, pH 5, 22 ± 2 °C)

t [min]	c_t [mg/L]	q_t [mg/g]	R [%]	t/q_t	$\ln(q_e - q_t)$
5	1,290 ± 85	66.0	11.3	0.076	6.24
10	1,029 ± 68	170	29.3	0.059	6.02
15	780 ± 51	270	46.4	0.056	5.74
30	555 ± 37	360	61.9	0.083	5.40
60	360 ± 24	438	75.3	0.137	4.97
90	110 ± 7	538	92.4	0.167	3.77
120	5.70 ± 3.76	580	99.6	0.207	0.610
960	1.10 ± 0.07	582	99.9	1.65	/*

* $\ln(q_e - q_t)$ could not be calculated due to $q_e \approx q_t$

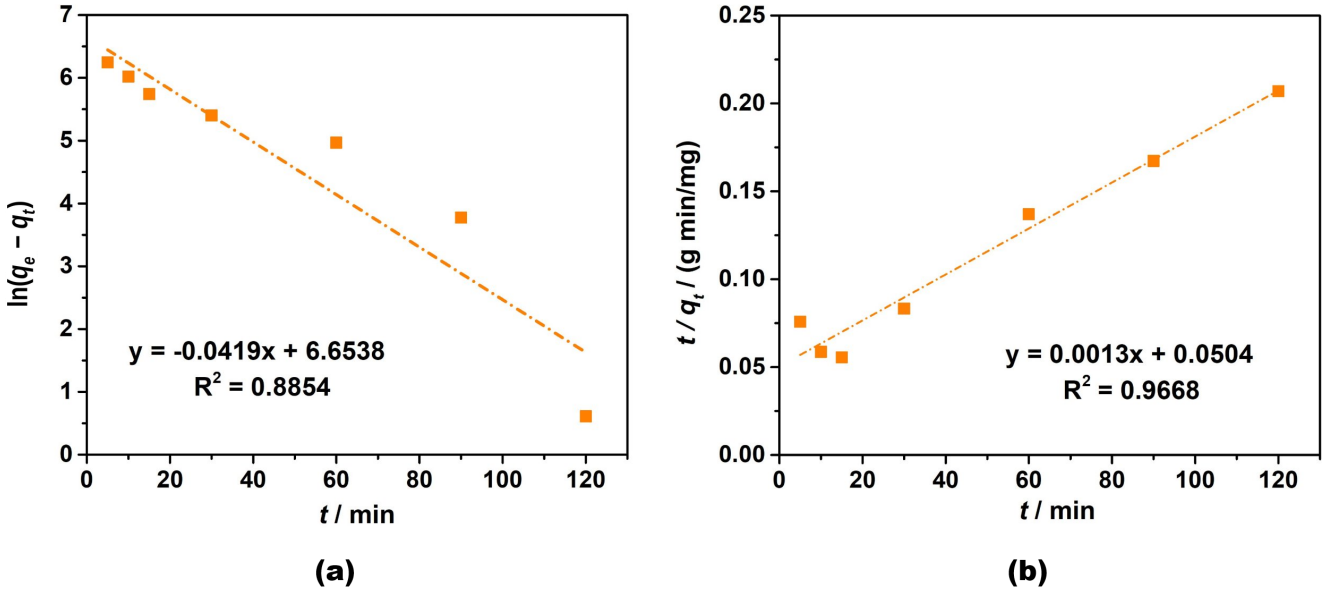


Fig. A1 Linear plots of the kinetic models of lead(II) adsorption on limestone: (a) pseudo-first-order (Eq. (6)); (b) pseudo-second-order (Eq. (7))

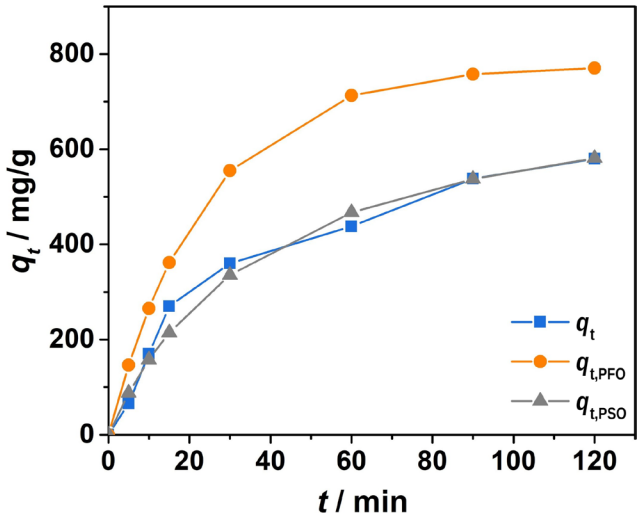


Fig. A2 Experimental data (q_t) and calculated curves for the pseudo-first-order ($q_{t,PFO}$) and pseudo-second-order ($q_{t,PSO}$) models of lead(II) adsorption on limestone

Table A4 Relative ratio of main XRD reflections of cerussite and calcite ($I_{24°}/I_{29°}$) at various adsorption times (t_{ads})

t_{ads} [min]	$I_{24°}/I_{29°}$
5	0.32
10	0.88
15	1.49
30	2.21
60	3.19
90	4.31
120	5.61
960	7.42